Available online at www.sciencedirect.com
ScienceDirect
Trans. Nonferrous Met. Soc. China 30(2020) 535−547
Transactions of Nonferrous Metals Society of China
www.tnmsc.cn

Preparation and performance of 3D-Pb anodes for nonferrous metals electrowinning in H_2SO_4 aqueous solution

Xiao-cong ZHONG[1,2,3], Bin ZHANG[1], Zhen-cong LIN[1], Jia-ming LIU[1], Yong-min XIE[1], Zhi-feng XU[1]

1. School of Metallurgical Engineering, Jiangxi University of Science and Technology, Ganzhou 341000, China;
2. Guangdong Institute of Rare Metals, Guangzhou 510650, China;
3. State Key Laboratory of Rare Metals Separation and Comprehensive Utilization, Guangzhou 510650, China

Received 24 June 2019; accepted 18 December 2019

Abstract: The effects of Pb^{2+} concentration, current density, deposition time and temperature on Pb deposit structure were investigated. In lower Pb^{2+} concentration (~0.15 mol/L), carambola-like 3D-Pb structure was constructed, while in higher Pb^{2+} concentration (≥0.30 mol/L), Pb deposits exhibited pyramid-like structure. Furthermore, the oxide layer and anodic potential of carambola-shaped 3D-Pb (Cara-Pb) and pyramid-shaped 3D-Pb (Pyra-Pb) anodes were investigated and compared with those of fresh Pb anode. After 72 h galvanostatic electrolysis (50 mA/cm^2) in 160 g/L H_2SO_4 solution, the oxide layer on Pyra-Pb was much thicker than that on Cara-Pb and Pb anodes, which remarkably relieved intercrystalline corrosion of the metallic substrate. Additionally, the oxide layer on Pyra-Pb anode presented a larger surface area and higher PbO_2 content. Hence, Pyra-Pb anode showed a 40 mV lower anodic potential compared to Cara-Pb and Pb anodes. In sum, Pyra-Pb anode had a potential to decrease energy consumption and prolong the life span of traditional Pb anode.

Key words: electrochemical deposition; 3D-Pb structure; growth mechanism; oxide layer; anodic potential

1 Introduction

Lead and lead alloys are used as traditional anodes in the electrowinning of nonferrous metals like zinc [1], copper [2], and manganese [3,4] from sulphate electrolytes. Lead/lead alloys are only used as initial anode materials since an oxide layer formed on the electrode surface works as actual reaction media after a long-stage electrolysis [5,6]. Fortunately, this oxide layer offers a lower current density and anode potential than fresh lead/lead alloys [7,8]. However, the oxide layer formed during electrolysis normally presents a porous coral-like structure and poorly adheres to the metallic substrate [9], which leads to corrosion of lead-based anodes and Pb-contamination of cathode products [10,11]. Therefore, the management of the oxide layer plays a pivotal role in enhancing anode performance in harsh working environment.

To improve the adhesion and stability of oxide layer on lead/lead alloy, RAMACHANDRAN et al [12] developed a method to create a hard dense PbO_2 layer on lead substrate by preconditioning the anode at high current density in an acidic fluoride-containing electrolyte. An alternative precondition process was developed by Mintek in the early 1990s, which involved sandblasting the surface of lead-base anodes with coarse silica sand at high pressures [3]. The sandblasting process could modify the surface texture, enlarge the surface area and enhance the adhesion of oxide layer [13].

Foundation item: Project (51704130) supported by the National Natural Science Foundation of China; Project (GK-201905) supported by the Research Fund of State Key Laboratory of Rare Metals Separation and Comprehensive Utilization, China; Project (jxxjbs16026) supported by the Doctoral Scientific Research Foundation of Jiangxi University of Science and Technology, China

Corresponding author: Zhi-feng XU; Tel: +86-797-8312204; E-mail: xzf_1@163.com

DOI: 10.1016/S1003-6326(20)65233-5

Afterwards, RST Technologies reported that a fine, uniform non-elongated grain structure of rolled lead alloys could facilitate the formation of a hard and dense PbO_2 layer [14], and the grain structure mentioned above could be obtained through controlling the rolling parameters. These cases demonstrated that surface modification was an adoptable strategy to improve the adhesion and stability of lead anodes.

Over the past 20 years, Ti/TiO_2 nanotube (NT) has been widely used in photocatalysis, dye-sensitized solar cells, and biomedical devices [15,16]. It was reported that in Ti/TiO_2 NT/PbO_2 for environmental applications, TiO_2 NT structure could act as an anchor for the PbO_2 deposits with better adherence and mechanical stability, consequently increasing by 3.5 times their life span with respect to Ti/PbO_2 anodes [17,18]. Enlightened by Ti/TiO_2 NT/PbO_2, in this work, 3D-Pb structure is constructed on Pb surface via electrochemical deposition. The introduction of 3D-Pb structure is aimed at improving the adhesion of oxide layer to Pb substrate during long term electrolysis, and further relieving the corrosion of lead anode. In this work, 3D-Pb anodes with carambola-like and pyramid-like structures were prepared. The growth behavior of 3D-Pb structure was discussed in detail. In addition, oxide layer property and anodic potential of these 3D-Pb anodes after/during 72 h galvanostatic electrolysis in 160 g/L H_2SO_4 solution were investigated and compared with fresh Pb anode.

2 Experimental

3D-Pb structures were constructed on 1 cm^2 fresh Pb substrate through galvanostatic electro-deposition. The basic compositions of the deposition bath were as follows: $Pb(BF_4)_2$, HBF_4, H_3BO_3 and gelatin [19,20]. All solutions were prepared with analytical reagents and deionized water. The electrodeposition experiments were conducted with a two-electrode system in 250 mL beaker. A graphite plate with an area of 4 cm^2 was used as counter electrode. The temperature of electrolyte was controlled through a thermostat (DF−101S). Pb substrates were ground to 1000 grit using a SiC abrasive paper and washed with deionized water before electrodeposition. The effects of Pb^{2+} concentration, current density, temperature, and deposition time on the morphologies of Pb deposits were investigated through scanning electron microscope (SEM, MIRA 3).

The electrochemical measurements on 3D-Pb anodes were performed in 160 g/L H_2SO_4 solution at (35±0.5) °C using a standard three-electrode system. A graphite plate of 4 cm^2 and Hg/Hg_2SO_4/sat. K_2SO_4 were used as counter and reference electrodes, respectively. All potentials shown in this study were relative to this reference electrode. To evaluate the performance of 3D-Pb anodes during metal electrowinning process, galvanostatic electrolysis was performed in 160 g/L H_2SO_4 solution at a current density of 500 A/m^2 for 72 h. During the galvanostatic electrolysis, anodic potentials were recorded by an electrochemical workstation (CH Instrument, 660E). After the galvanostatic electrolysis, linear scanning voltammetry (LSV) tests were immediately carried out. The scanning potential ranged from 1.45 to −1.50 V at a scanning rate of 5 mV/s. In terms of other samples in parallel tests, after 72 h galvanostatic electrolysis, the 3D-Pb anodes were taken out, washed with deionized water and dried for 8 h at 80 °C. Next, the surface and cross section morphology of 3D-Pb anodes were observed via SEM. The preparation method of cross section samples was illustrated in our previous work [21]. In addition, after surface morphology observation, the anodic layers on the surface of 3D-Pb anodes were removed by immersing in boiling solutions (100 g/L NaOH and 20 g/L glucose), and then the corrosion morphologies of metallic substrates were observed. Same experiments mentioned above have also been performed on fresh Pb anodes as comparison.

3 Results and discussion

3.1 Effect of Pb^{2+} concentration on Pb deposits structure

The surface morphologies of Pb deposits formed through galvanostatic electrodeposition in the presence of Pb^{2+} of different concentrations are presented in Fig. 1. As Fig. 1(a) shows, in the presence of 0.05 mol/L Pb^{2+}, only a small amount of Pb deposited on the surface during the given time, and the Pb deposits were relatively rough and porous. In solution containing 0.15 mol/L Pb^{2+}

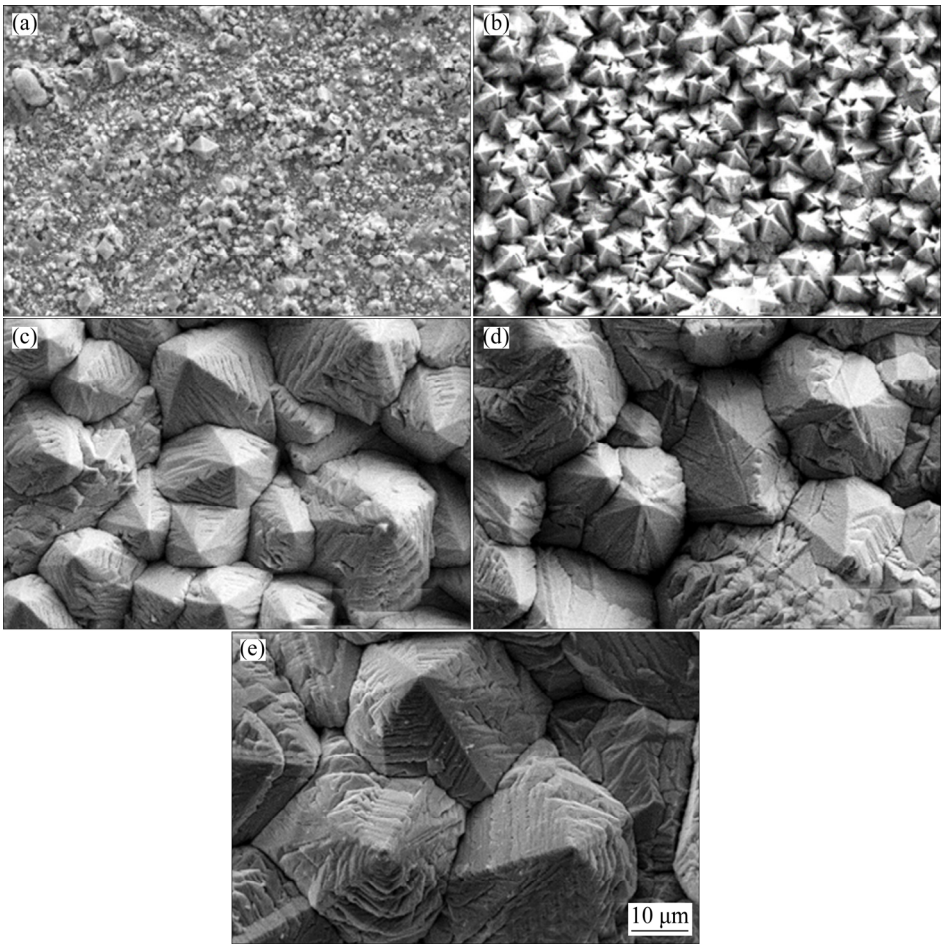

Fig. 1 Surface morphologies of Pb deposit formed through galvanostatic electrodeposition at 40 mA/cm^2 with different Pb^{2+} concentrations (deposition time: 40 min, temperature: 55 °C, and deposition bath composition: *x* mol/L $Pb(BF_4)_2$ + 0.40 mol/L HBF_4 + 12 g/L H_3BO_3 + 0.50 g/L gelatin): (a) *x*=0.05; (b) *x*=0.15; (c) *x*=0.30; (d) *x*=0.45; (e) *x*=0.60

(Fig. 1(b)), the Pb deposits exhibited a carambola-like structure. The substrate was entirely covered by evenly-distributed carambola-shaped Pb grains. The size of these carambola-shaped grains ranged from 1 to 5 μm. However, in the presence of higher Pb^{2+} concentration, the Pb deposits presented a quiet different structure. As observed in Fig. 1(c), the Pb grains presented a pyramid-like structure. More precisely, these pyramid-shaped Pb grains owned more than 4 arris lines. It was apparent that the size of pyramid-shaped Pb grains was much larger than carambola-shaped Pb grains. Further increasing Pb^{2+} concentration did not affect the Pb deposits structure obviously. As shown in Figs. 1(d, e), in the presence of 0.45 and 0.60 mol/L Pb^{2+}, the Pb deposits also presented a pyramid-like structure. As Pb^{2+} concentration in deposition bath increased, the grain size of pyramid-shaped Pb deposits increased apparently.

By comparing the surface morphologies of Pb deposits formed in the presence of Pb^{2+} of different concentrations, it is established that Pb^{2+} concentration exerted a critical effect on Pb deposits structure. When Pb^{2+} concentration of the deposition bath is higher than 0.05 mol/L, Pb deposits with 3D structures could be constructed. More specifically, the carambola-like Pb structure is obtained at a relatively lower Pb^{2+} concentration (~0.15 mol/L), while at a higher Pb^{2+} concentration (≥0.30 mol/L) Pb deposits tend to exhibit a pyramid-like structure.

As a 3D structure aimed at improving the adhesion and stability of oxide layer on metallic substrate, the Pb grain with 3D structure was expected to be uniform and robust mechanically. Hence, the effects of deposition parameters (current density, deposition time and temperature) on carambola-like and pyramid-like 3D-Pb structures

were further separately investigated in the presence of 0.15 mol/L and 0.30 mol/L Pb^{2+}.

3.2 Preparation of carambola-shaped 3D-Pb anode

3.2.1 Current density

Figure 2 depicts the surface morphologies of Pb deposits formed at different current densities in the presence of 0.15 mol/L Pb^{2+}. At current densities of 20 (Fig. 2(a)) and 40 mA/cm^2 (Fig. 2(b)), the Pb deposits both presented carambola-like structure. It was notable that some lumps were observed in the carambola-shaped grains in Fig. 2(a), while no apparent lump was seen in Fig. 2(b). Consequently, carambola-shaped grains formed at 40 mA/cm^2 seemed to be much more compact than that formed at 20 mA/cm^2. In addition, as current density increased, the Pb grain size decreased slightly. This rendered a larger number of carambola-shaped grains in Fig. 2(b) compared with Fig. 2(a). However, at 60 mA/cm^2, the Pb deposits were unexpectedly composed of a large number of bud-shaped grains (Fig. 2(c)). Therefore, to construct compact carambola-like 3D-Pb structure, a current density of 40 mA/cm^2 was preferable.

3.2.2 Deposition time

Figure 3 compares the surface morphologies of Pb deposits formed through different deposition time. After 10 min deposition (Fig. 3(a)), the Pb deposits presented bud-shaped structure, similar to what was observed in Fig. 2(c). This implied that the bud-shaped structure could be attributed to insufficient growth of Pb grains within short

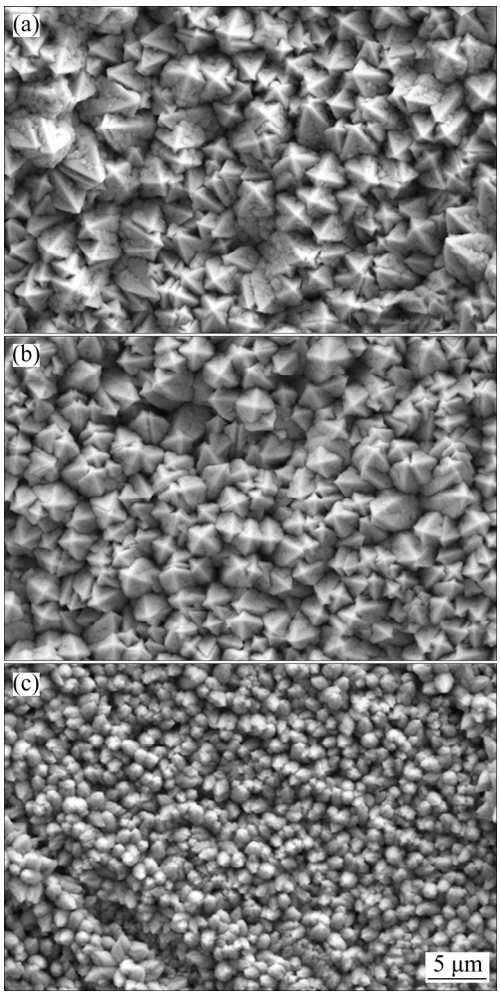

Fig. 2 Surface morphologies of Pb deposit formed through galvanostatic electrodeposition at different current densities (deposition time: 40 min, temperature: 35 °C and deposition bath composition: 0.15 mol/L $Pb(BF_4)_2$ + 0.40 mol/L HBF_4 + 12 g/L H_3BO_3 + 0.50 g/L gelatin): (a) 20 mA/cm^2; (b) 40 mA/cm^2; (c) 60 mA/cm^2

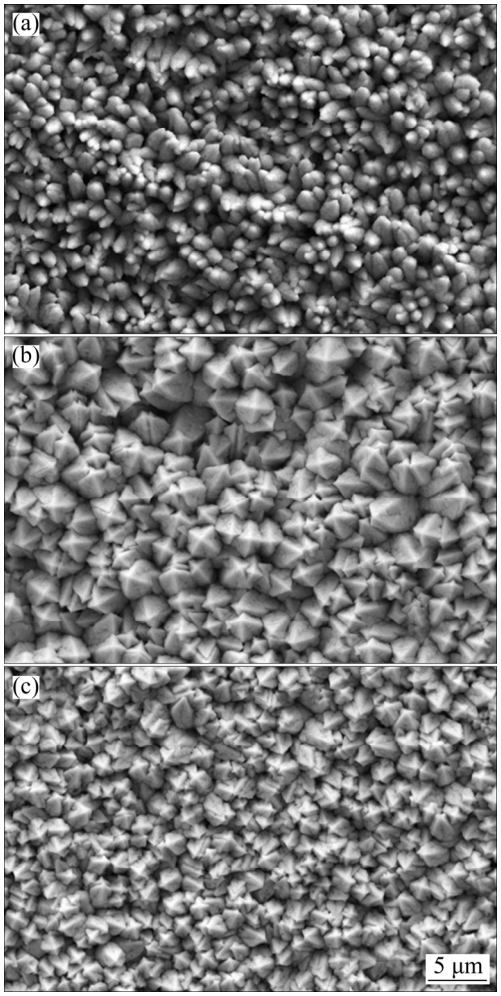

Fig. 3 Surface morphologies of Pb deposit formed through galvanostatic electrodeposition at 40 mA/cm^2 with different deposition time (temperature: 35 °C, and deposition bath composition: 0.15 mol/L $Pb(BF_4)_2$ + 0.40 mol/L HBF_4 + 12 g/L H_3BO_3 + 0.50 g/L gelatin): (a) 10 min; (b) 20 min; (c) 30 min

deposition time or at high current density. As deposition time prolonged, the Pb deposits tended to exhibit a regular carambola-like structure, as shown in Figs. 3(b, c). It was apparent that the grain size of Pb deposits formed through 30 min deposition was much smaller than that formed within 20 min. Consequently, the Pb deposit in Fig. 3(c) exhibited larger number of Pb grains and smaller height of Pb grains. As mentioned above, the 3D-Pb structure was expected to act as anchors to improve the adhesion of oxide layer. It was easy to understand that increasing the anchor length (height) was beneficial to improve the mechanical bonding strength between it and another subject due to a larger embedding depth. Hence, 3D-Pb structure shown in Fig. 3(c) might have limited anchor effect due to its small height. Therefore, the deposition time should be restricted to about 20 min.

3.2.3 Temperature

The surface morphologies of Pb deposits formed at different temperatures are shown in Fig. 4. Carambola-shaped Pb grains were observed at all investigated temperatures. It was apparent that as deposition temperature increased the grain size of carambola-shaped Pb deposit increased. At 55 °C, the Pb deposit presented highly uniform grain size (Fig. 4(c)). However, many lumps were observed in the Pb grains deposited at 45 and 55 °C. Especially at 45 °C, the presence of large number of lumps led to irregular and loose carambola-like structure, which would remarkably diminish its anchor function for oxide layer. Therefore, a lower deposition temperature was more adoptable in constructing carambola-like 3D-Pb structure. Additionally, it was found that in the presence of 0.15 mol/L Pb^{2+}, the lumps were more probable to exist in larger carambola-shaped Pb grains. Considering the limited anchor effect of Pb grain in small size or containing lumps, the grain size of carambola-shaped Pb deposits should be strictly controlled.

According to above results, it was demonstrated that the structure of Pb deposits was susceptible to deposition condition. Comparatively, the effects of current density and deposition time were more significant than deposition temperature. To obtain carambola-like 3D-Pb structure composed of compact and uniform Pb grains with preferable grain size, the deposition condition was optimized as follows: current density of 40 mA/cm^2, deposition time of 20 min, and deposition temperature of 35 °C. All carambola-shaped 3D-Pb anodes mentioned below were prepared under this condition.

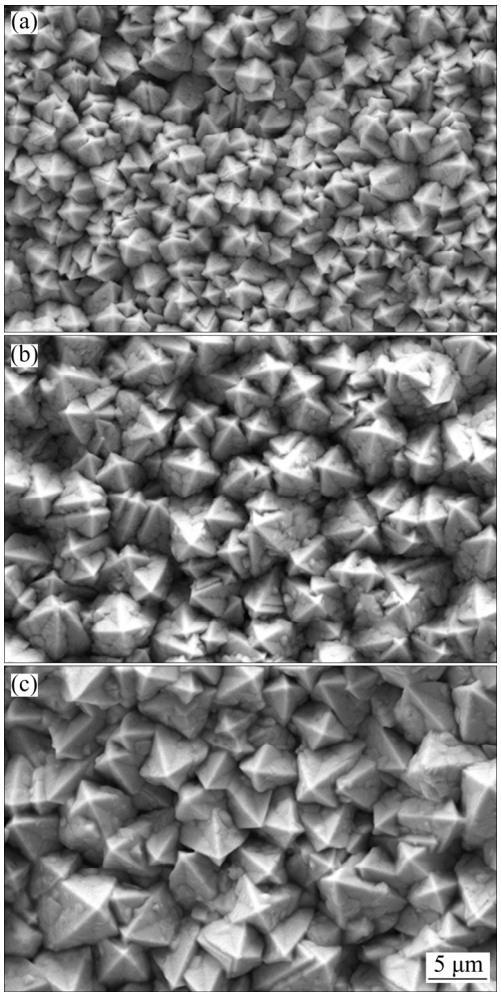

Fig. 4 Surface morphologies of carambola-shaped Pb deposit formed through galvanostatic electrodeposition at 40 mA/cm^2 and different temperatures (deposition time: 20 min, and deposition bath composition: 0.15 mol/L $Pb(BF_4)_2$ + 0.40 mol/L HBF_4 + 12 g/L H_3BO_3 + 0.50 g/L gelatin): (a) 35 °C; (b) 45 °C; (c) 55 °C

3.3 Preparation of pyramid-shaped 3D-Pb anode

3.3.1 Current density

The surface morphologies of Pb deposits formed in the presence of 0.30 mol/L Pb^{2+} at different current densities are shown in Fig. 5. At low current density (Fig. 5(a)), only a small part of Pb grains presented pyramid-like structure, and the height of these pyramid-shape Pb grains was small. Hence, the Pb deposits had a relatively smooth surface, which was detrimental to its anchor effect.

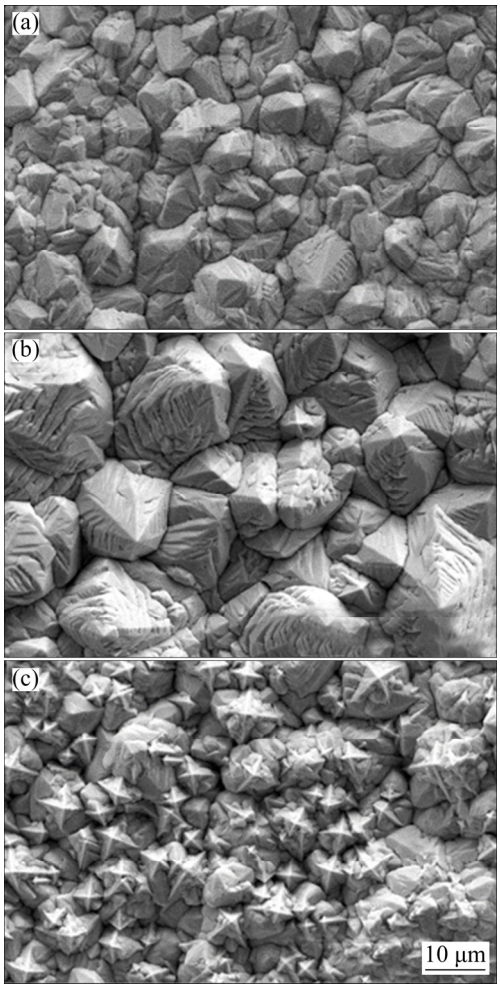

Fig. 5 Surface morphologies of pyramid-shaped Pb deposit formed through galvanostatic electrodeposition at different current densities (deposition time: 40 min, deposition bath composition: 0.30 mol/L $Pb(BF_4)_2$ + 0.40 mol/L HBF_4 + 12 g/L H_3BO_3 + 0.50 g/L gelatin, and deposition temperature: 55 °C): (a) 20 mA/cm^2; (b) 40 mA/cm^2; (c) 60 mA/cm^2

At 40 mA/cm^2 (Fig. 5(b)), most of Pb grains exhibited regular pyramid-like structure. However, at a higher current density (Fig. 5(c)), the Pb grains showed different structures in different regions. The Pb grains near the substrate mainly presented irregular pyramid-like structure, while a large number of carambola-shaped Pb grains were observed on the surface of these irregular pyramid-shaped Pb grains. The appearance of carambola-shaped Pb grains could be explained by low Pb^{2+} concentration at the deposition frontline due to severe depletion of Pb^{2+} during galvanostatic deposition at high current density.

3.3.2 Deposition time

Figure 6 compares surface morphologies of Pb deposits formed through different deposition time. It was apparent that deposition time also had a significant effect on Pb deposits structure. After 10 min (Fig. 6(a)), the pyramid-shaped Pb grains failed to entirely cover the substrate. In addition, the Pb deposit presented a relatively smooth surface

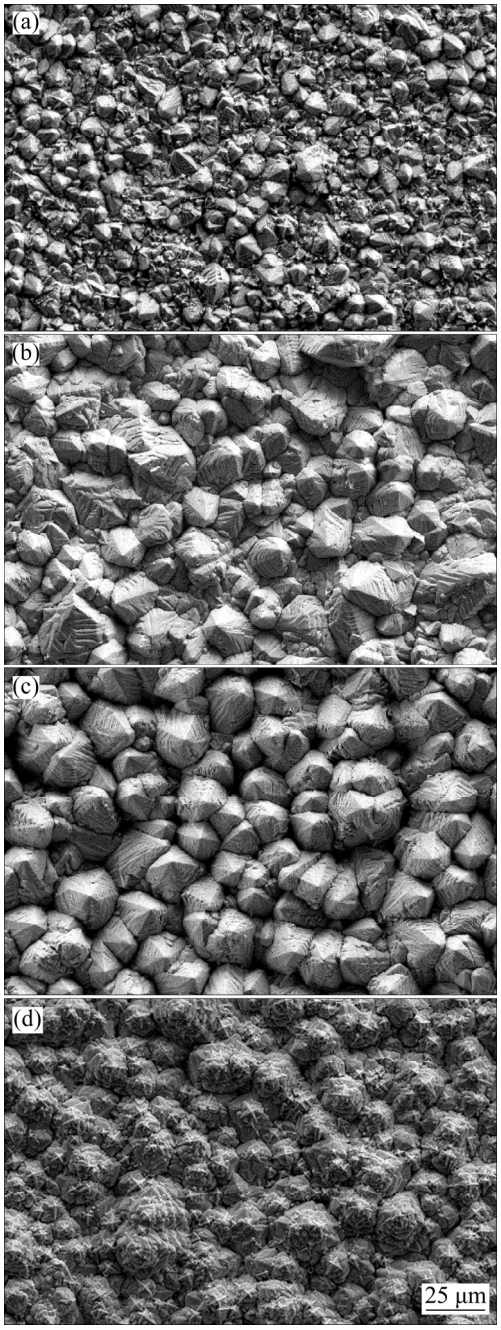

Fig. 6 Surface morphologies of pyramid-shaped Pb deposit formed through galvanostatic electrodeposition at 40 mA/cm^2 with different deposition time (deposition temperature: 55°C, and deposition bath composition: 0.30 mol/L $Pb(BF_4)_2$ + 0.40 mol/L HBF_4 + 12 g/L H_3BO_3 + 0.50 g/L gelatin): (a) 10 min; (b) 20 min; (c) 40 min; (d) 60 min

due to small height of Pb grains. When the deposition time was prolonged (Figs. 6(b, c)), the density and height of pyramid-shaped Pb grains increased gradually. As shown in Fig. 6(c), the deposited Pb grains exhibited regular pyramid-like structure with an average size of 30 μm. However, further prolonging deposition time led to amorphous deposits on the surface (Fig. 6(d)). Therefore, deposition time of 40 min was preferable to construct pyramid-like 3D-Pb structure.

3.3.3 Temperature

Figure 7 depicts the surface morphologies of Pb deposits formed at different temperatures. Similar to the effect of temperature on the surface morphologies of carambola-like 3D-Pb structure, the size of pyramid-shaped Pb grains increased as deposition temperature increased. Simultaneously, the density and height of exposed pyramid-shaped Pb grains decreased, which would be detrimental to the anchor function of pyramid-like 3D-Pb structures. Especially at 55 °C (Fig. 7(c)), due to the larger Pb grain size, the interspace among pyramid-shaped Pb grains substantially decreased, so was the exposure height of pyramid-shaped Pb grains. Therefore, the deposition temperature was optimized to be 35 °C to obtain preferable pyramid-like 3D-Pb structure.

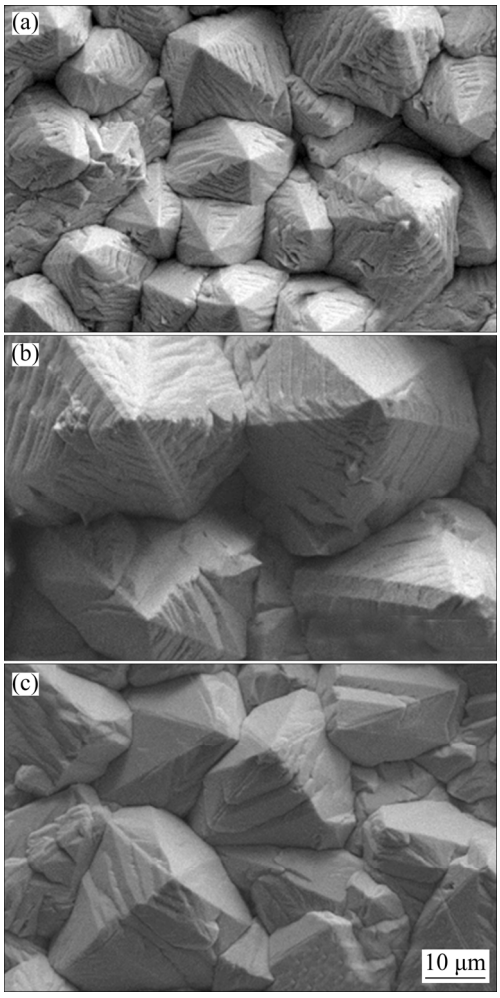

Fig. 7 Surface morphologies of pyramid-shaped Pb deposit formed through galvanostatic electrodeposition at 40 mA/cm^2 and different temperatures (deposition time: 40 min, and deposition bath composition: 0.30 mol/L $Pb(BF_4)_2$ + 0.40 mol/L HBF_4 + 12 g/L H_3BO_3 + 0.50 g/L gelatin): (a) 35 °C; (b) 45 °C; (c) 55 °C

Similar to carambola-shaped Pb deposit, the structure of pyramid-shaped Pb deposit was also susceptible to deposition condition. The size, density and height of Pb grains could be regulated by controlling current density, deposition time and temperature. The optimized deposition condition was as follows: current density of 40 mA/cm^2, deposition time of 40 min, and deposition temperature of 35 °C. All pyramid-shaped 3D-Pb anodes mentioned below were prepared under this condition.

3.4 Deposition behavior of Pb^{2+}

It has been demonstrated that Pb^{2+} concentration, current density, deposition temperature and deposition time all affect the structure of Pb deposits. Especially, the Pb deposits structure is most susceptible to Pb^{2+} concentration, implying that Pb deposition process is largely determined by Pb^{2+} mass transport. As deposition proceeded, the Pb^{2+} concentration at the deposition frontline depleted in different extents. Hence, the Pb^{2+} deposition rate in different directions varied due to different Pb^{2+} concentration gradients between deposition frontline and bulk solution. To better understand the correlation between Pb deposit structure and initial Pb^{2+} concentration, it was assumed that in the presence of a specific Pb^{2+} concentration (marked as C_a) the Pb deposit presented normal pyramid shape as shown in Fig. 8(a). In the case that Pb^{2+} initial concentration in deposition bath was lower than C_a, the Pb^{2+} deposition behaviors in different directions were analyzed separately. In the direction vertical to the substrate, the deposition rate at the apex was the largest due to the sufficient supply of Pb^{2+} through almost spherical diffusion. However, in the plane parallel to the substrate, the deposition rates in different directions were represented by the length of blue arrows shown in Fig. 8(b). The deposition

rate was inversely proportional to the distance between deposition site and adjacent arris line. Namely, at the middle point between two arris lines Pb^{2+} deposited at the slowest rate, while at the arris line the Pb^{2+} deposited at the fastest rate. This could be explained by the smaller number of deposition sites and larger amount of available bulk solution in the region near arris line. Due to the various deposition rates in different directions as analyzed above, the Pb deposits transferred from pyramid-like structure to carambola-like structure. In the case of high Pb^{2+} concentration ($>C_a$) in deposition bath (Fig. 8(c)), the mass transport of Pb^{2+} was much faster due to larger Pb^{2+} concentration gradient. In the plane parallel to the substrates, the number of preferable deposition directions for Pb^{2+} deposition might increase, which could result in pyramid-shaped Pb grain with more arris lines (>4), as observed in Figs. 1(c−e). Furthermore, it could be speculated that if Pb^{2+} concentration in deposition bath was sufficiently high (Fig. 8(d)), the Pb^{2+} deposition rate would be the same in different directions in the plane parallel to the substrate. Consequently, the Pb deposit would exhibit cone-shaped structure.

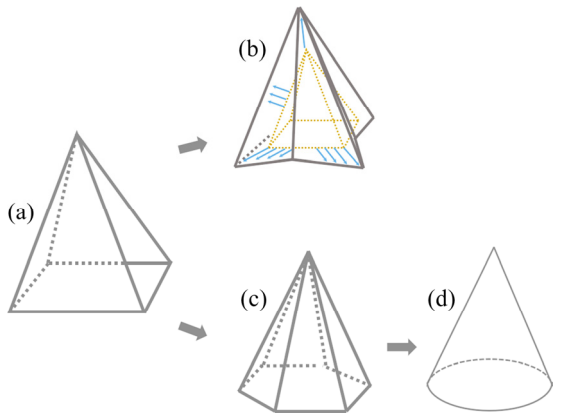

Fig. 8 Schematic presentation of transformation of Pb deposit structure as function of initial Pb^{2+} concentration in deposition bath: (a) Pyramid-like structure; (b) Carambola-like structure; (c) Polygonal pyramid-like structure; (d) Cone-shaped structure

3.5 Characterization of oxide layer on 3D-Pb anodes

During the metal electrowinning process, a constant current is placed on lead-based anodes. As electrowinning process proceeds, an oxide layer mainly containing PbO_2 and $PbSO_4$ formed gradually on the surface. This oxide layer not only acted as a barrier to protect the metallic substrate from continuous attack by electrolyte, but also provided active sites for oxygen evolution reaction. Therefore, the properties of oxide layer play a vital role in the performance of lead-based anode. In this work, surface morphology, cross-section morphology and composition of oxide layer were characterized.

3.5.1 Surface morphology

Surface morphologies of the oxide layer formed on 72 h polarized Pb, carambola-shaped 3D-Pb (designated as Cara-Pb) and pyramid-shaped 3D-Pb (designated as Pyra-Pb) anodes are presented in Fig. 9. As shown in Fig. 9(a), some cracks were observed in the oxide layer of 72 h polarized Pb anode. The oxide layer near these cracks was rough and porous, presenting a typical coral-like structure. However, in other regions, the

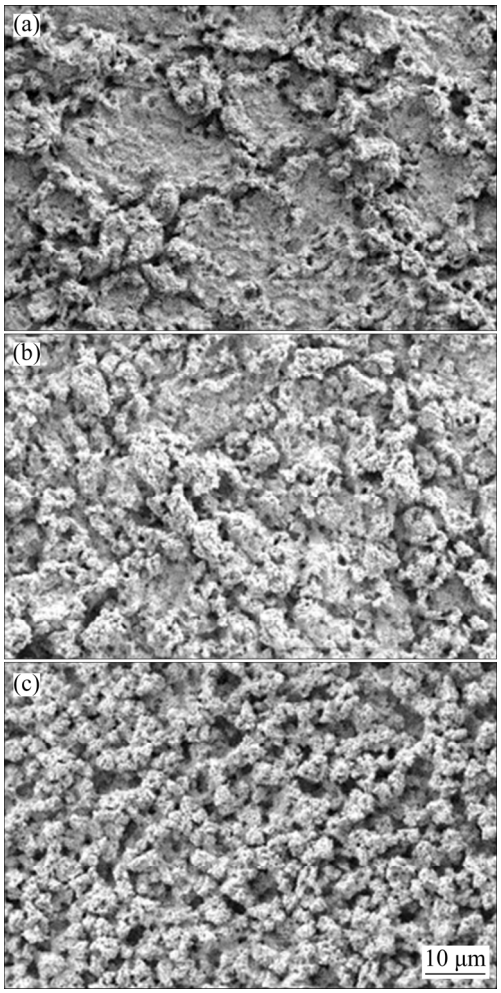

Fig. 9 Surface morphologies of oxide layer formed on surface of Pb (a), Cara-Pb (b), and Pyra-Pb (c) anodes after 72 h galvanostatic electrolysis in 160 g/L H_2SO_4 solution at 50 mA/cm^2 and 35 °C

oxide layer was relatively smooth and compact. These cracks would not provide sufficient protection to the metallic substrate, which may lead to permeation of electrolyte and corrosion of Pb substrate [22,23]. In the case of Cara-Pb (Fig. 9(b)) and Pyra-Pb (Fig. 9(c)) anodes, the oxide layer presented similar coral-like structure. However, there was no obvious crack observed on these two anodes. This denoted that carambola-like and pyramid-like 3D structures were beneficial to improving the integrity of oxide layer on Pb anodes. Compared with Cara-Pb anode, the oxide layer on Pyra-Pb anode was much rougher and presented abundant pores. Due to these pores distributed in the oxide layer, the actual surface area of polarized Pyra-Pb anode was much larger than that of Pb and Cara-Pb anodes.

3.5.2 Cross-section morphology

As a physical barrier between metallic substrate and electrolyte, the inner structure of oxide layer plays a crucial role in the performance of lead-based anodes [21,24]. To clarify the effect of 3D-Pb structure on the inner structure of oxide layer, the cross-section morphologies of 72 h polarized Pb, Cara-Pb and Pyra-Pb anodes were observed via back scattered electron imaging. As shown in Fig. 10, the cross-section images could be divided into three sections. The black section on the top represented the insulate resin, the white section at the bottom indicated the metallic substrate, and the gray section between the black and white sections corresponded to the oxide layer [21]. In Fig. 10(a), the surface of oxide layer on polarized Pb anode was relatively compact and smooth, which matched with the surface morphology shown in Fig. 9(a). Its thickness was about 10 μm. As for polarized Cara-Pb anode (Fig. 10(b)), its thickness was close to that of the polarized Pb anode. However, the oxide layer was rougher and less compact compared to that of polarized Pb anode, which could be attributed to the typical coral structure of oxide layer, as observed in Fig. 9(b). As shown in Fig. 10(c), the cross-section of oxide layer on polarized Pyra-Pb anode was quite different from that on polarized Pb and Cara-Pb anodes. Firstly, its thickness was about 60 μm, far greater than what was observed in Figs. 10(a, b). Secondly, the oxide layer surface was much rougher and more porous than that of polarized Pb and Cara-Pb anodes, which seemed like tree branch. This could be explained by the presence of abundant pores, as observed in Fig. 9(c). A cracking was observed in the oxide layer shown in Fig. 10(c), probably due to either high stress levels in the oxide layer or drying process, which was common in thick coatings [25,26]. Fortunately, the inner part of oxide layer on polarized Pyra-Pb anode was compact and integral, which would provide sufficient protection for the underneath metallic substrate.

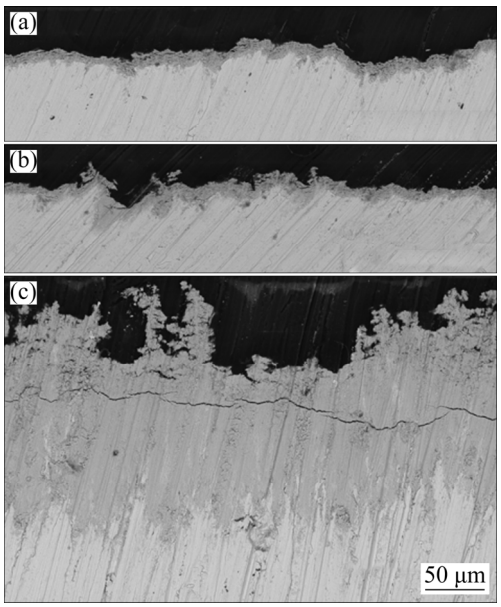

Fig. 10 Cross-sectional images of Pb (a), Cara-Pb (b) and Pyra-Pb (c) anodes after 72 h galvanostatic electrolysis in 160 g/L H_2SO_4 solution at 50 mA/cm^2 and 35 °C

3.5.3 Composition

Cathodic linear sweep voltammetry (LSV) was performed to analyze the composition of oxide layer formed during 72 h galvanostatic electrolysis. As shown in Fig. 11, the first cathodic peak (denoted as A) of the LSV curves appeared in the potential range of 0.50−1.00 V. This cathodic peak could be attributed to the reduction of PbO_2 to $PbSO_4$ [27,28]. It was apparent that Peak A of polarized Pyra-Pb anode presented much higher peak intensity and larger peak area, demonstrating that more PbO_2 was formed during the 72 h electrolysis. Another cathodic peak (denoted as B) was observed on the voltammograms of polarized Pb and Cara-Pb anodes, representing the reduction of PbO, $PbO{\cdot}PbSO_4$ and $PbSO_4$ [29]. However, Peak B was not observed on polarized Pyra-Pb anode. It could be inferred that at the end of LSV test, the oxide layer on polarized Pyra-Pb anode

was not entirely reduced. This resulted in a reduction branch rather than Peak B on the LSV curve of polarized Pyra-Pb anode. This result matched with the thicker oxide layer as proven in Fig. 10(c). Therefore, it was confirmed that the pyramid-shaped 3D-Pb structure facilitated the formation of PbO_2 in the oxide layer.

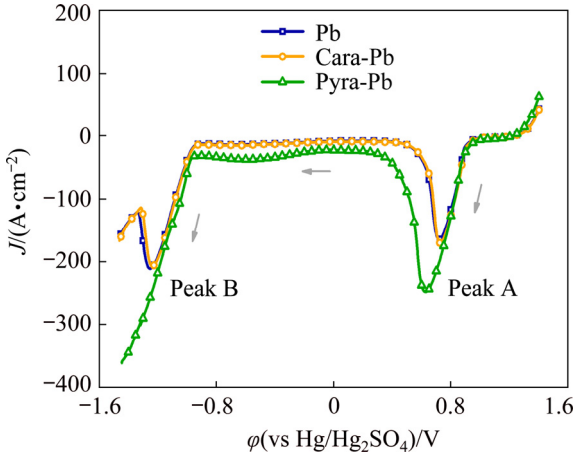

Fig. 11 Cathodic linear sweep voltammetry curves of Pb, Cara-Pb and Pyra-Pb anodes after 72 h galvanostatic electrolysis with potential from 1.45 to −1.50 V at 5 mV/s and 35 °C

3.6 Corrosion morphology of 3D-Pb anodes

Figure 12 compares corrosion morphologies of 72 h-polarized Pb, Cara-Pb and Pyra-Pb anodes after removing the oxide layers by chemical dissolution method. As shown in Figs. 12(a, b), metallic substrates of Pb and Cara-Pb anodes presented evident intercrystalline corrosion, which was also reported by MOHAMMADI et al [22]. The intercrystalline corrosion was the most likely reason for the appearance of cracks in the oxide layer on 72 h-polarized Pb anodes, as seen in Fig. 9(a). In the intercrystalline corrosion region, the formation of corrosion products was faster than in other regions. Consequently, higher inner pressure in this region led to the appearance of pores and cracks in the oxide layer. Compared with Pb anode, the depth of corrosion crack on Cara-Pb anode was smaller, implying the positive effect of carambola- like 3D-Pb structure on corrosion resistance of Pb anodes, which was in line with the absence of cracks in the oxide layer shown in Fig. 9(b). However, the appearance of corrosion cracks in Fig. 12(b) revealed that the carambola-like structure was destroyed after 72 h electrolysis. This could demonstrate that carambola-like structure

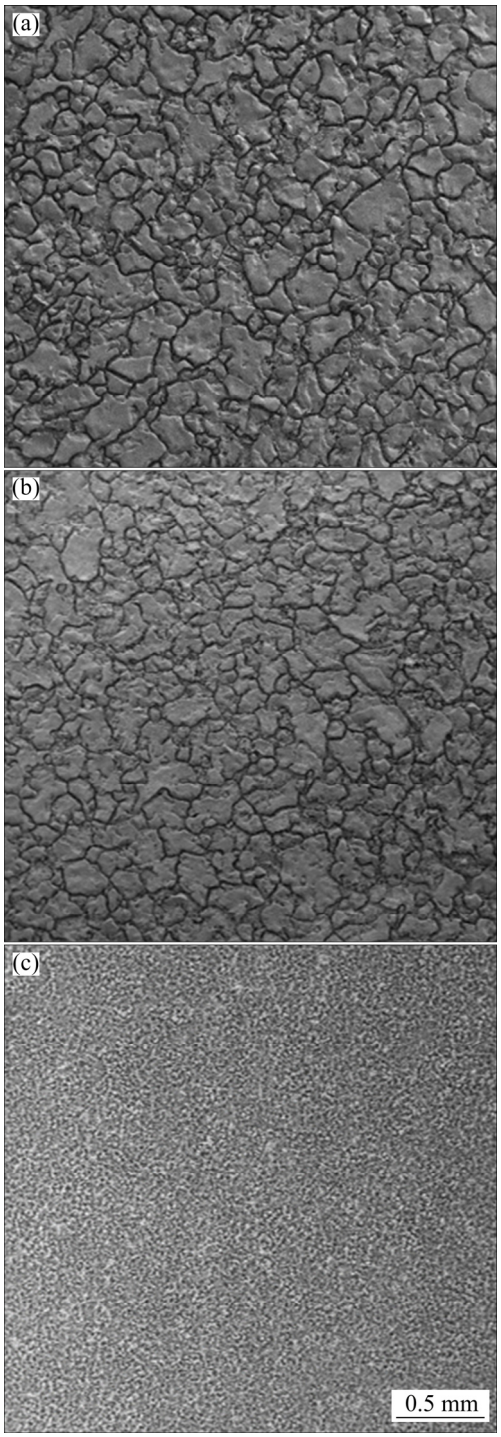

Fig. 12 Corrosion morphologies of Pb (a), Cara-Pb (b), and Pyra-Pb (c) anodes after 72 h galvanostatic electrolysis in 160 g/L H_2SO_4 solutions at 50 mA/cm^2 and 35 °C

only had a short-term function. Unlike what was observed on Pb and Cara-Pb anodes, there was no obvious corrosion cracks observed on the metallic substrate of Pyra-Pb anode (Fig. 12(c)), suggesting that the corrosion process remained undergoing in the pyramid-shaped Pb deposits. Namely, the

corrosion did not yet extend to the pristine Pb substrate. This could be explained that the larger thickness of oxide layer provided sufficient protection for the underneath metallic substrate from electrolyte attack. The results mentioned above demonstrated that pyramid-like 3D-Pb structure was more beneficial to prolonging the life span of Pb anode.

3.7 Anodic potential of 3D-Pb anodes

At the beginning of galvanostatic electrolysis, growth of oxide layer and oxygen evolution reaction (OER) proceeded simultaneously on lead anodes. The effects of 3D-Pb structures on the growth of oxide layer and OER over time were investigated using galvanostatic polarization. These experiments were performed at a constant current density of 50 mA/cm^2, which was adopted in a typical zinc tank house. Anodic potential variations of Pb, Cara-Pb and Pyra-Pb anodes during 72 h galvanostatic electrolysis are shown in Fig. 13.

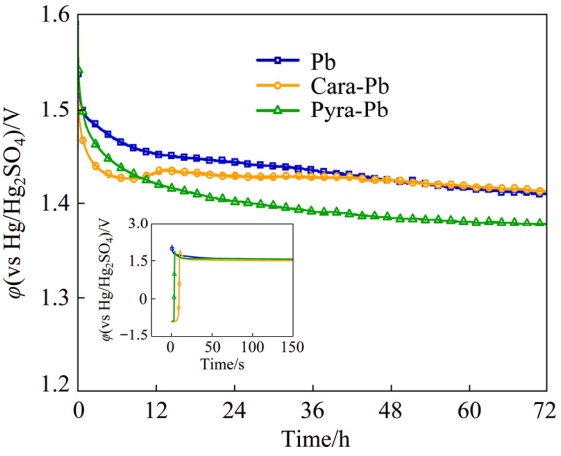

Fig. 13 Anodic potential variations of Pb, Cara-Pb and Pyra-Pb anodes during 72 h galvanostatic electrolysis in 160 g/L H_2SO_4 solutions at 50 mA/cm^2 and 35 °C

Inset in Fig. 13 shows the potential variation during the initial 150 s. A rapid decline of anodic potential was observed on Pb anodes when the electrolysis began, while the anodic potential of Cara-Pb and Pyra-Pb anodes ascended drastically at the beginning. The potential ascending could be attributed to the longer charging time of double electronic layer on 3D-Pb anodes due to their larger surface area. It can be inferred that Cara-Pb anode had a larger surface area because of its longer charging time compared with Pyra-Pb anode. Afterwards, anodic potential of three anodes descended substantially due to rapid formation of PbO_2 on the surface.

As shown in Fig. 13, at initial 12 h, Cara-Pb anode presented the lowest anodic potential, which could be explained by the depolarization effect of its largest surface area. However, the potential of Cara-Pb exhibited a slight increase after 10 h, which might be attributed to the decreasing of surface area due to the growth of oxide layer in the grain interspace. After 15 h, anodic potential of three anodes descended continuously. At 70 h, the potentials tended to level off due to a relatively stable anodic layer formed on the surface. It could be observed that the potential−time curves of Pb and Cara-Pb anodes almost overlapped at the end of 72 h electrolysis. While the anodic potential of Pyra-Pb anode was about 40 mV lower than that of Pb and Cara-Pb anodes. Based on the characterization of oxide layer, the lower anodic potential of Pyra-Pb anode could be attributed to larger surface area of oxide layer and higher PbO_2 content formed during 72 h galvanostatic electrolysis. As demonstrated by MONAHOV and PAVLOV [30,31], the PbO_2 was a prerequisite for the formation of OER active sites. Both large surface area and higher PbO_2 content facilitated the formation of OER active sites. Therefore, it could be concluded that the pyramid-like 3D-Pb structure was beneficial to improving OER reactivity. Due to the lower anodic potential, Pyra-Pb anode had a great capacity to decrease the energy consumption of the metal electrowinning process.

4 Conclusions

(1) In lower Pb^{2+} concentration (~0.15 mol/L), carambola-like 3D-Pb structure could be constructed, while in higher Pb^{2+} concentration (≥0.30 mol/L), Pb deposits tended to exhibit pyramid-like structure. The 3D-Pb structures could be modified by adjusting current density, deposition time and temperature.

(2) Both carambola-like and pyramid-like 3D-Pb structures were beneficial to improving integrity of oxide layer formed during long-stage electrolysis. The oxide layer on Pyra-Pb anode had a larger actual surface area and higher PbO_2 content, which rendered Pyra-Pb anode a lower anodic potential.

(3) Both carambola-like and pyramid-like

3D-Pb structures were beneficial to relieving the intercrystalline corrosion of Pb anodes. Due to the thicker oxide layer formed during electrolysis, there was no obvious corrosion crack observed on Pyra-Pb anode after 72 h electrolysis. Thus, Pyra-Pb anode was expected to possess a longer life span.

(4) Pyra-Pb anode was demonstrated to have the potential to decrease anodic potential and prolong life span of Pb anodes. When applied in metal electrowinning industry, Pyra-Pb anode was expected to decrease energy consumption and capital cost of the electrowinning process.

References

[1] JIN Lei, HUANG Hui, YANG Fei, YANG Hai-tao, ZHANG Hong-yan, GUO Zhong-cheng. Polymer anode used in hydrometallurgy: Anodic behaviour of PANI/CeO_2/WC anode from sulfate electrolytes [J]. Hydrometallurgy, 2018, 176: 201−207.

[2] ZHANG Wei, ROBICHAUD M, GHALI E, HOULACHI G. Electrochemical behavior of mesh and plate oxide coated anodes during zinc electrowinning [J]. Transactions of Nonferrous Metals Society of China, 2016, 26(2): 589−598.

[3] WANG Wen-jun, WANG Zuo-ran, YUAN Tie-chui, LI Rui-di, LI Hai-hua, LIN Wen-jun, ZHENG Dan. Oxygen evolution and corrosion behavior of Pb−CeO_2 anodes in sulfuric acid solution [J]. Hydrometallurgy, 2019, 183: 221−229.

[4] ZHOU Xiang-yang, WANG Shuai, YANG Juan, GUO Zhong-cheng, YANG Jian, MA Chi-yuan, CHEN Bu-ming. Effect of cooling ways on properties of Al/Pb−0.2%Ag rolled alloy for zinc electrowinning [J]. Transactions of Nonferrous Metals Society of China, 2017, 27(9): 2096−2103.

[5] HU Gang, XU Rui-dong, HE Shi-wei, CHEN Bu-ming, YANG Hai-tao, YU Bo-hao, LIU Qiang. Electrosynthesis of Al/Pb/α-PbO_2 composite inert anode materials [J]. Transactions of Nonferrous Metals Society of China, 2015, 25(6): 2095−2102.

[6] LI Y, JIANG L, LI J, LIU Y. Novel phosphorus-doped lead oxide electrode for oxygen evolution reaction [J]. RSC Advances, 2014, 4(11): 5339−5342.

[7] YANG H, GUO Z, CHEN B, LIU H, ZHANG Y, HUANG H, LI X, FU R, XU R. Electrochemical behavior of rolled Pb−0.8%Ag anodes in an acidic zinc sulfate electrolyte solution containing Cl^- ions [J]. Hydrometallurgy, 2014, 147: 148−156.

[8] IVANOV I, STEFANOV Y, NONCHEVA Z, PETROVA M, DOBREV T, MIRKOVA L, VERMEERSCH R. Insoluble anodes used in hydrometallurgy: Part II. Anodic behaviour of lead and lead-alloy anodes [J]. Hydrometallurgy, 2000, 57(2): 125−139.

[9] MOHAMMADI M, ALFANTAZI A. Anodic behavior and corrosion resistance of the Pb−MnO_2 composite anodes for metal electrowinning [J]. Journal of the Electrochemical Society, 2013, 160(6): C253−C261.

[10] MA R, CHENG S, ZHANG X, LI S, LIU Z, LI X. Oxygen evolution and corrosion behavior of low-MnO_2-content Pb−MnO_2 composite anodes for metal electrowinning [J]. Hydrometallurgy, 2016, 159: 6−11.

[11] MOHAMMADI F, TUNNICLIFFE M, ALFANTAZI A. Corrosion assessment of lead anodes in nickel electrowinning [J]. Journal of The Electrochemical Society, 2011, 158(12): C450−C460.

[12] RAMACHANDRAN P, NAGANATHAN K, BALAKRISHNAN K, SRINIVASAN R. Effect of pretreatment on the anodic behaviour of lead alloys for use in electrowinning operations. I [J]. Journal of Applied Electrochemistry, 1980, 10(5): 623−626.

[13] FREE M, MOATS M, ROBINSON T, NEELAMEGGHAM N, HOULACHI G, GINATTA M, CREBER D, HOLYWELL G. Electrometallurgy-now and in the future [C]//TMS 2012 Annual Meeting. Orlando, 2012: 3−28.

[14] PRENGAMAN R D, SIEGMUND A. New wrought Pb−Ag−Ca anodes for zinc electrowinning to produce a protective oxide coating rapidly [C]//Lead-zinc 2000 Symposium. Warrendale, PA, 2000: 589−596.

[15] ZHOU X, LIU S, YU H, XU A, LI J, SUN X, SHEN J, HAN W, WANG L. Electrochemical oxidation of pyrrole, pyrazole and tetrazole using a TiO_2 nanotubes based SnO_2−Sb/3D highly ordered macro-porous PbO_2 electrode [J]. Journal of Electroanalytical Chemistry, 2018, 826: 181−190.

[16] LIU J, XIAO S, SHEN Z, XU L, ZHANG L. Study on the oxidative stabilization of polyacrylonitrile fibers by microwave heating [J]. Polymer Degradation and Stability, 2018, 150: 86−91.

[17] MOURA D, QUIROZ M, SILVA D, SALAZAR R, MARTÍNEZ-HUITLE C. Electrochemical degradation of acid blue 113 dye using TiO_2-nanotubes decorated with PbO_2 as anode [J]. Environmental Nanotechnology, Monitoring & Management, 2016, 5: 13−20.

[18] XU M, WANG Z, WANG F, HONG P, WANG C, OUYANG X, ZHU C, WEI Y, HUN Y, FANG F. Fabrication of cerium doped Ti/nanoTiO_2/PbO_2 electrode with improved electrocatalytic activity and its application in organic degradation [J]. Electrochimica Acta, 2016, 201: 240−250.

[19] LAI Y, LI Y, JIANG L, LV X, LI J, LIU Y. Electrochemical performance of a Pb/Pb−MnO_2 composite anode in sulfuric acid solution containing Mn^{2+} [J]. Hydrometallurgy, 2012, 115: 64−70.

[20] LAI Y, LI Y, JIANG L, XU W, LV X, LI J, LIU Y. Electrochemical behaviors of co-deposited Pb/Pb−MnO_2 composite anode in sulfuric acid solution–Tafel and EIS investigations [J]. Journal of Electroanalytical Chemistry, 2012, 671: 16−23.

[21] ZHONG X, WANG R, XU Z, JIANG L, LV X, LAI Y. Influence of Mn^{2+} on the performance of Pb−Ag anodes in fluoride/chloride-containing H_2SO_4 solutions [J]. Hydrometallurgy, 2017, 174: 195−201.

[22] MOHAMMADI M, MOHAMMADI F, HOULACHI G, ALFANTAZI A. The role of electrolyte hydrodynamic properties on the performance of lead-based anodes in electrometallurgical processes [J]. Journal of the Electrochemical Society, 2013, 160(3): E27−E33.

[23] ZHONG Xiao-cong, CHEN Fang-hui, WANG Rui-xiang, XU Zhi-feng. A Review on the stability of lead-based anodes in H_2SO_4 solution [J]. Materials Reports, 2019, 33(9): 2862−2867. (in Chinese)
[24] ZHANG C, LIU J, CHEN B. Effect of CeO_2 and graphite powder on the electrochemical performance of Ti/PbO_2 anode for zinc electrowinning [J]. Ceramics International, 2018, 44(16): 19735−19742.
[25] MOHAMMADI M, ALFANTAZI A. The performance of Pb−MnO_2 and Pb−Ag anodes in 2 Mn(II)-containing sulphuric acid electrolyte solutions [J]. Hydrometallurgy, 2015, 153: 134−144.
[26] ZHONG Xiao-cong, WANG Rui-xiang, LIU Qing-sheng, JIANG Liang-xing, LAI Yan-qing, LI Jie. Effects of fluoride and chloride ions on anodic layer and corrosion behavior of Pb−Ag anode [J]. The Chinese Journal of Nonferrous Metals, 2018, 28(4): 792−801. (in Chinese)
[27] SHARPE T. The behavior of lead alloys as PbO_2 electrodes [J]. Journal of the Electrochemical Society, 1977, 124(2): 168−173.
[28] LI R, ZHOU J, LIU J, CHEN B. Effects of current density on preparation and performance of Al/α−PbO_2−CeO_2−TiO_2 composites [J]. Materials Research Express, 2019, 6(7): 075802.
[29] SUN Q, GUO Y. Effects of antimony on the formation process of $3PbO{\cdot}PbSO_4{\cdot}H_2O$ on Pb and Pb-Sb electrodes [J]. Journal of the Electrochemical Society, 2000, 493: 123−129.
[30] MONAHOV B, PAVLOV D. Hydrated structures in the anodic layer formed on lead electrodes in H_2SO_4 solution [J]. Journal of Applied Electrochemistry, 1993, 23: 1244−1250.
[31] PAVLOV D. The lead-acid battery lead dioxide active mass: A gel-crystal system with proton and electron conductivity [J]. Journal of the Electrochemical Society, 1992, 139(11): 3075−3080.

硫酸体系有色金属电沉积用 3D-Pb 阳极的制备与性能

钟晓聪[1,2,3]，张 斌[1]，林振聪[1]，刘嘉铭[1]，谢永敏[1]，徐志峰[1]

1. 江西理工大学 冶金工程学院，赣州 341000；
2. 广东省稀有金属研究所，广州 510650；
3. 稀有金属分离与综合利用国家重点实验室，广州 510650

摘 要：研究 Pb^{2+}浓度、电流密度、沉积时间和温度对沉积 Pb 结构的影响。在低 Pb^{2+}浓度条件下(~ 0.15 mol/L)，Pb 沉积物呈杨桃状，而在高 Pb^{2+}浓度条件下(≥0.30 mol/L)，Pb 沉积物呈立锥状。进一步对比研究杨桃状 Pb 阳极(Cara-Pb)、立锥状 Pb 阳极(Pyra-Pb)和 Pb 阳极的氧化膜层和阳极电位。在 160 g/L H_2SO_4 溶液中恒流极化(50 mA/cm^2) 72 h 后，Pyra-Pb 阳极氧化膜层厚度大于 Cara-Pb 和 Pb 阳极，进而显著减缓金属基底的晶界腐蚀。此外，Pyra-Pb 阳极氧化膜层具有更大表面积和更高 PbO_2 含量，因此，极化 72 h 后 Pyra-Pb 阳极电位较 Cara-Pb 和 Pb 阳极的低 40 mV。综上，在 Pb 阳极表面构建立锥状 3D-Pb 结构具有降低电沉积能耗、延长阳极寿命的潜力。

关键词：电化学沉积；3D 铅结构；生长机理；氧化膜层；阳极电位

(Edited by Bing YANG)